α cluster structures in unbound states in ^{19}Ne

Reiji Otani[1], Masataka Iwasaki[1], and Makoto Ito[1,a]

[1]*Department of Pure and Applied Physics, Kansai University, 3-3-35 Yamatecho, Suita, Osaka 564-8680, Japan.*

Abstract. Cluster structures in ^{19}Ne are studied by the microscopic and macroscopic cluster models. In the microscopic calculation, the coupled-channels problem of (^{3}He+^{16}O) + (α+^{15}O) is solved, and the adiabatic energy surfaces, which are the series of the energy eigenvalues as a function of the He–O distance, are investigated. In the adiabatic energy curves, the several local minima are generated in the spatial region of the small core distance, where the neutron hole inside of the He or O nucleus is strongly coupled to the residual nuclei. The energy spectra, which are constructed from the strong coupling states, nicely reproduce the the low-lying energy levels in the ^{19}Ne nucleus. In the macroscopic approach, the α + ^{15}O potential is evaluated from the elastic scattering of the α + ^{15}N system, and the resonant levels of the α + ^{15}O system are calculated under the absorbing boundary condition. The potential model predicts the existence of the resonances above the α threshold, which has a weak-coupling scheme of the α particle and one hole inside of the ^{16}O nucleus. The extended microscopic calculations of (^{3}He+^{16}O) + (α+^{15}O) + (^{5}He+^{14}O) are performed in order to see the coupling effect of the $5p$-$2h$ configuration, which corresponds to the shell model limit of the ^{5}He + ^{14}O cluster configuration. The extended calculation suggests that the ^{5}He + ^{14}O configuration plays an important role on the formation of the $3/2^+$ resonance at 0.5 MeV with respect to the α threshold.

1 Introduction

The α cluster structures have been extensively studied for the so-called $4N$ nuclei with $N = Z$, such as ^{8}Be = 2α, ^{12}C = 3α, ^{16}O = α + ^{12}C, and ^{20}Ne = α + ^{16}O [1–3]. In current studies, the importance of the cluster degrees of freedom has been extended to the neutron-rich ($N > Z$) systems, which are obtained by adding extra neutrons to the $4N$ cluster systems. In the neutron-rich systems, such as ^{12}Be = 2α + $4N$ [4], ^{16}C = 3α + $4N$ [5] and ^{22}Ne = α + ^{16}O + $2N$ [6], various chemical-bonding-like structures are generated by the coupling of the cluster relative motion and the single particle motion of extra neutrons. In particular, the drastic structure changes among the chemical bonding-like states are pointed out in the continuum energy region of ^{12}Be [4].

On the contrary, cluster structures in the $4N$ systems with a hole in a cluster core, are also interesting research subjects [7–11]. For example, there is a recent study of ^{11}B = α + α + t, corresponding to a proton hole system of ^{12}C = 3α [7]. Pioneering work of the hole system is the study of the ^{19}F nucleus [8–11]. The ^{19}F nucleus is the one proton deficient system of ^{20}Ne, and the rotational bands

_____

[a]e-mail: itomk@kansai-u.ac.jp

of α + ^{15}N and t + ^{16}O, which are calculated from the folding type potential, were clearly assigned to the energy levels observed in the α and t transfer reactions [8]. The energy levels in ^{19}F have also been analyzed in the more sophisticated models, such as the full microscopic α + ^{15}N cluster model on the basis of the generator coordinate method (GCM) [9, 10] and the orthogonalized condition model (OCM) of the (t + ^{16}O) + (α + ^{15}N) coupled-channels [11]. In the coupled-channels analysis, t and α cluster bands are clearly identified although a considerable mixture of these two configurations occurs.

In the previous analyses on ^{19}F [9, 11], the so-called weak coupling states of the proton hole are confirmed above the α threshold energy. For example, in the α + ^{15}N system, a proton hole inside of the ^{16}O cores loosely couples to the relative motion of the binary cluster cores. In a naive consideration, the weak coupling state of the hole in ^{16}O and the α particle is also expected in the neutron-deficient system, α + ^{15}O in ^{19}Ne [10, 11]. In fact, a formation of α + ^{15}O in ^{19}Ne was discussed from the perspective of ^{19}F – ^{19}Ne Coulomb displacement energy [8, 11]. However, detailed analysis of the energy levels over a wide energy region, which covers the unbound continuum states, the analysis of the resonance width above the α threshold and the excitation function of the resonant scattering, have not been undertaken yet because available experimental data are still limited. Therefore, a study of the α + ^{15}O cluster structure in ^{19}Ne, corresponding to the $N < Z$ system, is very interesting from the viewpoint of the systematics of the clustering phenomena in the $N \neq Z$ systems.

Recently, we have applied the potential model to the α + ^{15}O system [12] and predicted the existence of the resonances, which have the weak coupling feature, above the α threshold. The potential model is useful to understand the resonant states, in which the α clustering is well developed. However, the microscopic cluster model, in which the anti-symmetrization among the nucleons are completely performed, is very important in analyzing the energy levels from the low-lying states to the highly-excited states in a unified manner. In particular, the anti-symmetrization effect is essential for the low-lying states, which is difficult to handle in the potential model. In the present report, we apply the microscopic cluster model of (^{3}He + ^{16}O) + (α + ^{15}O) and mainly analyze the low-lying states in ^{19}Ne. The microscopic model and the potential model are combined to analyze the levels from the low-lying region to the highly-excited region.

There is another reason why we focus on the α + ^{15}O structure in the ^{19}Ne nucleus. The ^{15}O(α,γ)^{19}Ne reaction is known to play a crucial role in the advanced stages of astrophysical hydrogen burning [13]. In the ^{15}O(α,γ)^{19}Ne reaction, the most crucial resonance is known to arise through the $J^{\pi} = 3/2^+$ resonant level at 504 keV with respect to the α + ^{15}O threshold ($E_x = 4.03$ MeV). Unfortunately, direct measurement of the resonance at 504 keV is still difficult because of the small strength of the resonance and its energy position extremely close to the α decay threshold. The analyses in Ref. [14] have pointed out that the intrinsic structure of the resonance at 504 keV in ^{19}Ne is not the α + ^{15}O cluster structure, but the five particle–two hole (5p–2h) shell-model configuration with the ^{14}O$_{g.s.}$ core. The 5p–2h configuration has a large overlap with the shell model limit of the ^{5}He + ^{14}O configuration. Therefore, the coupling of ^{5}He + ^{14}O on the $J^{\pi} = 3/2^+$ state is essential in the cluster model approach. In this report, the result of the extended microscopic calculation of (^{3}He+^{16}O) + (α+^{15}O) + (^{5}He+^{16}O) in $J^{\pi} = 3/2^+$ will also be reported.

2 Framework

2.1 microscopic cluster model

We apply the generalized two-center cluster model (GTCM) for the calculations of the low-lying levels [4]. The GTCM is the extended model of the microscopic cluster model on the basis of the generator coordinate method (GCM) [15]. The application of GTCM to Be isotopes ($\alpha + \alpha + N + N$

+...) has already been published in Ref. [4], and we briefly explain the formulation of GTCM in the ^{19}Ne nucleus. The basis function for ^{19}Ne is given by

$$\Phi^{J^\pi K}(S) = \hat{P}_K^{J^\pi} \mathcal{A} \left\{ \psi(^3\text{He})\psi(^{14}\text{O}) \prod_{j=1}^{2} \varphi_j(m_j) \right\}_S . \tag{1}$$

The basis function is constructed on the basis of ^{3}He + ^{14}O cores, and the two neutrons are treated as the active valence-nucleons. The $\psi(^3\text{He})$ and $\psi(^{14}\text{O})$ represent the core wave functions of the ^{3}He and ^{14}O nuclei, respectively. The former part is described by the $(0s)^3$ configuration in the harmonic oscillator (HO) potential, while the latter part is constructed by the $(0s)^4(0p)^{10}$ configuration. Two centers are placed with the relative distance parameter S, which is treated as the generator coordinate. The single-particle wave function for the j-th valence neutrons ($j = 1, 2$) localized around the ^{3}He or ^{14}O clusters is given by an atomic orbital (AO) $\varphi(m_j)$, which is classified by a set of the AO quanta $m_j = (k, C, \tau)$ with the labels of the HO orbitals k, the core C, and the neutron spin τ (= ↑ or ↓). The HO orbitals around the core C ($C = {}^3$He or ^{14}O) are $k = 0s$ ($C = {}^3$He) or $k = 0p$ ($C = {}^{14}$O). The basis functions with the full anti-symmetrization $\mathcal{A}$ are projected to the eigenstate of the total spin J, its intrinsic angular projection K, and the total parity π by the projection operator $\hat{P}_K^{J^\pi}$.

The total wave function is finally given by taking the superposition over S, **m** and K as

$$\hat{\Psi}_\nu^{J^\pi} = \int dS \sum_{\mathbf{m},K} C_{\mathbf{m}K}^{J^\pi \nu}(S) \Phi_{\mathbf{m}}^{J^\pi K}(S) . \tag{2}$$

The coefficients $C_{\mathbf{m}}^{J^\pi \nu}(S)$ in Eq. (2) for the ν-th eigenstate are determined by solving a coupled channel GCM (Generator Coordinate Method) equation [15]

$$\left\langle \Phi_{\mathbf{m}}^{J^\pi}(S) \mid \hat{H} - E_\nu^{J^\pi} \mid \Psi_\nu^{J^\pi} \right\rangle = 0 . \tag{3}$$

Here $\hat{H}$ and $E_\nu^{J^\pi}$ denote the total Hamiltonian and the energy eigenvalues of the ν-th eigenstate for the J^π state, respectively. Before solving Eq. (3), we can investigate the structure changes with respect to the variation of the ^{3}He–^{14}O distance parameter. Namely, we solve the eigenvalue problem at a fixed S, such as

$$(\hat{H} - E_\mu^{J^\pi}(S)) \Phi_{AS}^{J^\pi \mu}(S) = 0 \tag{4}$$

with

$$\Phi_{AS}^{J^\pi \mu}(S) = \sum_{\mathbf{m}K} D_{\mathbf{m}K}^{J^\pi \mu}(S) \Phi_{\mathbf{m}K}^{J^\pi \mu}(S) . \tag{5}$$

The μ-th eigenvalue $E_\mu^{J^\pi}(S)$ is a function of the relative distance-parameter S, and a sequence of $E_\mu^{J^\pi}(S)$ forms the energy surfaces. The energies $E_\mu^{J^\pi}(S)$ and wave functions $\Phi_{AS}^{J^\pi \mu}(S)$ correspond to the so-called "adiabatic energy surfaces (AESs)" and "adiabatic states (ASs)", respectively, in atomic physics [4]. The detailed properties of AESs and ASs are reported in Ref. [4].

As for the nucleon-nucleon (NN) interaction, we use the Volkov No.2 [16] and the G3RS [17] for the central and spin-orbit parts, respectively. The parameters in the NN interactions and the size parameter of HO are tuned to reproduce the ^{3}He and ^{4}He decay threshold of ^{19}Ne as much as possible. In the present calculation, the HO size parameter is set to $b = 1.6$ fm, while the strength of the Volkov No. 2 are taken to be ± 60 MeV without Bartlett and Heisenberg terms ($B = H = 0$). This parameter setting is the same as the previous microscopic calculation in ^{19}F [10]. We have found that the strength of Majorana term (M) must be varied depending on the parity: $M = 0.638$ for the positive parity and $M = 0.62$ for the negative parity. The feature of the parity dependence is also similar to the previous study of ^{19}F in Ref. [10]. The strength of the G3RS is taken to be ±1500 MeV, which is the same order of the magnitude as the analysis of Be isotopes [4].

2.2 Macroscopic cluster model

The macroscopic potential model is also applied to calculate the unbound resonant states [12]. In the unbound resonances, the mean distance of α–^{15}O is expected to be enhanced, and two nuclei are weakly coupled. In the treatment of the weak coupling scheme, the potential model is quite useful. The Woods Saxon (WS) potential is assumed for the nuclear potential in α + ^{15}O, and its parameter set is fixed so as to reproduce the angular distribution of the α + ^{15}N elastic scattering.

In the determination of the parameters, the scattering problem of α + ^{15}N is solved in the range of $E_\alpha = 23.7 \sim 55$ MeV. In the scattering calculation, the complex WS potential is employed, and we consider only the central part of the complex potential. The WS parameters of the real part is fixed over a whole energy range of the scattering calculation, while the parameters in the imaginary part are set to be energy dependent. The resultant WS potential reproduces the feature of the folding type potential, which used in the analysis of ^{20}Ne = α + ^{16}O [18].

The resonant levels of α + ^{15}O are calculated from the α + ^{15}N potential by adding the Coulomb and spin-orbit potentials. The strength of the spin-orbit potential is chosen to reproduce the energies of the bound levels of the $5/2^-$ and $3/2^-$ states, which are considered to be the pair levels in the spin-orbit splitting. Above the α decay threshold, the absorbing boundary condition (ABC) [19] is applied to identify the resonant levels, having the resonance energy E_R and the decay width Γ_R. The detailed explanations of the potential model plus ABC is shown in Ref. [12].

3 Results

3.1 Adiabatic energy curves

First, we solve Eq. (5) for the coupled channels of (^{3}He+^{16}O) + (α+^{15}O) and calculate the adiabatic energy surfaces (AESs). In Figure 1, the AESs with $J^\pi = 3/2^+$ are shown. In the AESs, the structure change from the two-body weak-coupling states to the one-body strong-coupling states occurs as the distance parameter S gets smaller. The vertical dashed line at $S = 6.5$ fm represents the boundary of the weak-coupling states and the strong-coupling states. Here, we call this boundary distance S_C.

At the outside region of S_C, the He and O nuclei slip to each other with the internal spins ($1/2^-$ or $3/2^-$ for ^{15}O and $1/2^+$ for ^{3}He) and the relative spin of L. In the particle-hole picture, the neutron hole in ^{16}O (α) weakly couples to the residual nucleus, α (^{16}O). On the contrary, in the small distance of $S_C \leq 6.5$ fm, the effect of the nuclear interaction begins to be strong. The effect of the nu-

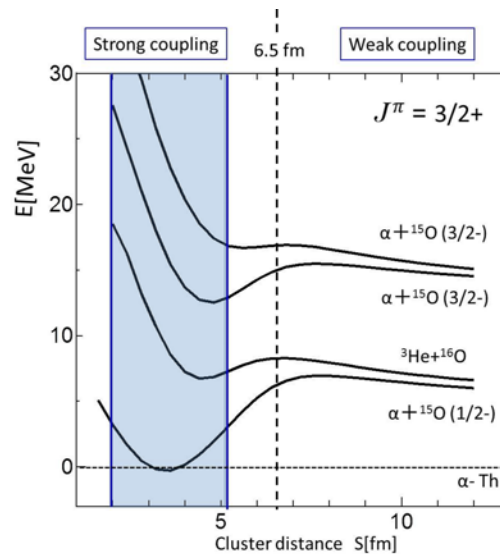**Figure 1.** Adiabatic energy curves calculated from the coupled channels of (^{3}He+^{16}O) + (α+^{15}O). The abscissa and ordinate represent the He–O distance and the excitation energy measured from the α threshold energy (horizontal dotted line). See text for details.

clear interaction leads to the strong mixture of the weak coupling states. The mixture of the weak

coupling states corresponds the so-called strong coupling states, in which neutron holes are difficult to move inside of a nucleus freely, and the holes tend to be fixed to a certain spatial direction.

In the region of the strong coupling scheme, the local minima appear in the individual energy curves. This means that the energy levels respective to the energy minima are generated when we solve the coupled-channel GCM equation (3). In the present GCM calculation, the range of the distance parameter is set to $S = 2 \sim 5.2$ fm, which covers the local minima in the strong coupling region, as shown by the shaded area in Fig. 1. Therefore, the main components of the resultant energy levels are the strong coupling states, in which the neutron holes are tightly bound around the residual nuclei. Thus, the weak coupling states are excluded in the present computational space.

The weak coupling states are also possible to appear in the energy levels if the range of the distance parameter is extended in the GCM calculation. However, the weak coupling states are mainly appear as the resonant states in the continuum energy region and hence, the consideration of the scattering boundary condition is important in the careful analysis of the weak coupling states. The analysis of the the weak coupling states under the scattering boundary condition is a future subject [4].

3.2 Energy spectra

In Fig. 2, the energy spectra for the negative parties are plotted. The microscopic GCM spectra of the (^{3}He+^{16}O) + (α+^{15}O) at the middle position are compared with the experimental data plotted at the left side. The microscopic calculation reproduce the level ordering of the low-lying experimental spectra up to the α threshold (dashed line). The $7/2^-$ state becomes the bound state in the microscopic calculation, while the respective level in experiment, the spin of which is tentatively assigned, is resonant state just above the α threshold. This failure may be improved by tunning the parameters in the NN interaction and extending the range of the distance parameter S.
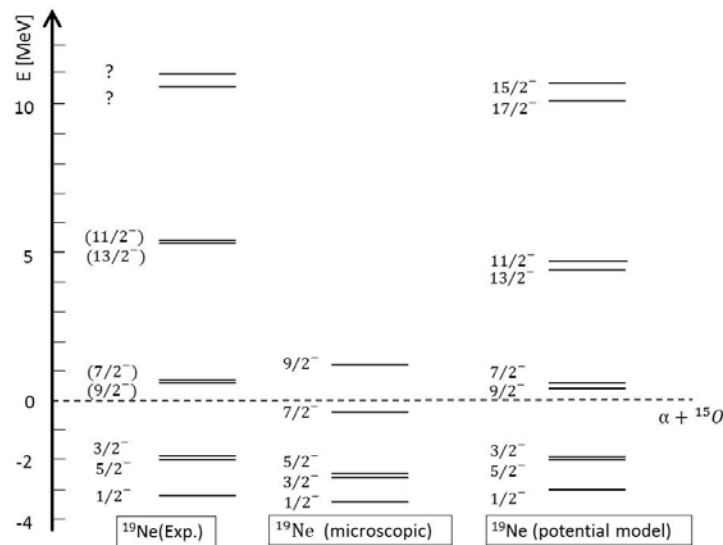

Figure 2. Energy levels of the negative parity states in ^{19}Ne. The left levels are the experimental data, while middle and right levels are the results of the microscopic and macroscopic models, respectively. The dotted line represents the α threshold energy, which is set to the zero energy.

The right side levels are the results of the potential model. In the potential model calculation, the low-lying bound levels are fairly reproduced. Furthermore, the potential model under the absorbing boundary condition (ABC) predicts the resonant levels above the α threshold. The resonant width is not shown for simplicity although the width are calculated in the ABC treatment. Unfortunately, the experimental information is still insufficient in the unbound region. Thus, the experimental investigation of the highly-excited states are strongly desired.

The result of the positive parity states are shown in Fig. 3. The microscopic GCM calculation with $(^3\text{He}+^{16}\text{O}) + (\alpha+^{15}\text{O})$ is shown at the center position, while the experimental levels are plotted at the left position. The GCM calculation nicely reproduces the energy levels of the bound states below the α threshold although the energy position of the $7/2^+$ state is a little higher than the experimental observation. At the right side, the spectra obtained by the potential model are plotted in the unbound region above the α threshold, but the respective experiment is still insufficient. The resonance width and the excitation function of the resonant α scattering are predicted in Ref. [12]. Thus, the future experiments on the unbound resonances are very interesting.

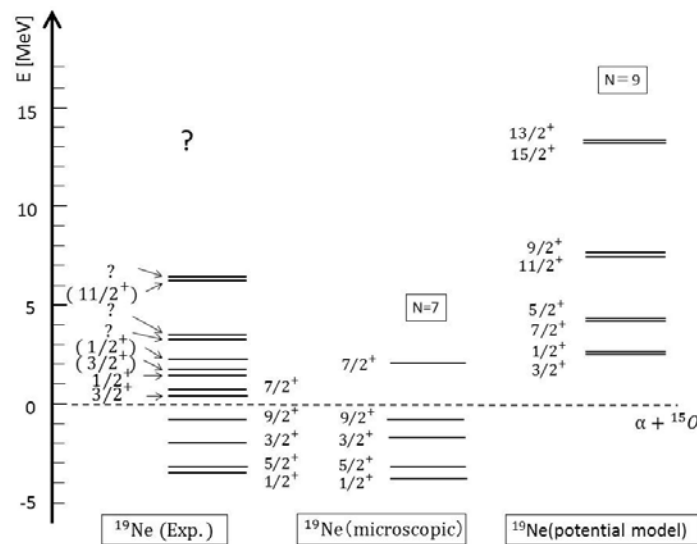**Figure 3.** Same as Fig. 2 except for the positive parity states in ^{19}Ne.

The relative wave function of the $\alpha+^{15}\text{O}$ cluster configuration in the potential model (right levels) corresponds to the HO states with the total oscillator quantum number of $N = 9$, which is the same as the negative parity band in the $^{20}\text{Ne} = \alpha + ^{16}\text{O}$ system [18]. On the contrary, the microscopic calculation is one lower nodal state with $N = 7$. In the potential model, the $3/2^+$ state becomes a ground state with $N = 7$, and its binding energy is about -11 MeV with respect to the α threshold. Therefore, the potential model does not reproduce the properties of the ground and low-lying levels below the α threshold, which are the member of the $N = 7$ state. This is because the He and O nuclei are strongly overlapped in the $N = 7$ state, where the anti-symmetrization effect among the nucleons becomes strong. In the potential model, the anti-symmetrization effect is not completely taken into account and hence, the binding energies of the $N = 7$ states are deeper than the energies of the experimental levels.

The positive parity levels in Fig. 2 and the negative parity levels in Fig. 3 are belong to the $N = 8$ and $N = 9$ states, respectively, which correspond to the higher nodal state of $N = 7$. In these higher nodal states, the mean distance of the He and O clusters is much more enhanced than the distance in the $N = 7$ states, and the anti-symmetrization effect is not so effective. Therefore, the potential model nicely works in describing the experimental data corresponding to the higher nodal levels. The potential model is successful in handling the higher nodal states but the microscopic calculation is very important in the unified analysis of the energy spectra over a wide energy region.

3.3 Effect of the ^{5}He + ^{14}O configuration

In the result shown in Fig. 3, we can confirm that the $3/2^+$ state just above the α threshold is missing in both the microscopic and macroscopic calculations. This failure is the same as the results of the previous microscopic GCM calculation of ^{19}F $= \alpha + {}^{15}$N [10] and the coupled-channel OCM calculation in ^{19}F $= ({}^3$H$+{}^{16}$O$) + (\alpha+{}^{15}$N) [11]. Therefore, the α and ^{3}He cluster configurations are considered to be minor component in the threshold $3/2^+$ state. This result is consistent to the previous experimental result, which points out the dominance of the $5p$–$2h$ configuration in the threshold $3/2^+$ state [14], because the α and ^{3}He cluster configurations have the large overlap with the $4p$–$1h$ and $3p$–$0h$ shell model configurations, respectively, in the $S = 0$ limit. Therefore, we should include other cluster configuration, which has a large overlap of the $5p$–$2h$ state.
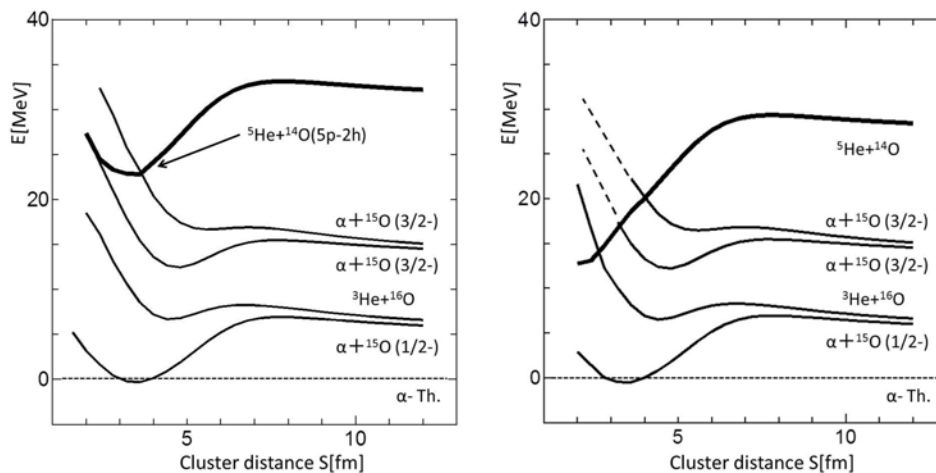

Figure 4. Adiabatic energy curves calculated by the coupled channels of $({}^3$He$+{}^{16}$O$) + (\alpha+{}^{16}$O$) + ({}^5$He$+{}^{14}$O$)$. The left panel shows the truncated calculation, in which the $5p$–$2h$ configuration is mainly considered for ^{5}He $+ {}^{14}$O, while the full calculation is shown in the right panel. In both panels, the thick curves correspond to the solutions with the dominant ^{5}He$+{}^{14}$O channels. See text for details.

The ^{5}He $+ {}^{14}$O configurations are the possible configuration, which has a large overlap of the $5p$–$2h$ state. In order to improve the calculation for the $3/2^+$ state, we have also performed the extended microscopic calculation, which is the coupled-channels of $({}^3$He$+{}^{16}$O$) + (\alpha+{}^{16}$O$) + ({}^5$He$+{}^{14}$O$)$, to include the $5p$–$2h$ configuration in the shell model limit ($S = 0$). The total number of the ^{5}He $+ {}^{14}$O configurations is 36. The computational process is divided into two stages. First, we truncate the

model space of ^{5}He + ^{14}O to the specific 16 channels, which mainly change into the $5p$–$2h$ configurations in the $S = 0$ limit. The truncated $5p$–$2h$ channels are included in the extended calculation of (^{3}He+^{16}O) + (α+^{16}O) + (^{5}He+^{14}O). Secondly, the full model space is included in the calculation with the three partitions.

In Fig. 4, the adiabatic energies are shown for the truncated calculation (left panel) and the complete calculation (right panel). In the left panel, the thick curve shows the energy curve of the ^{5}He + ^{14}O configuration, while the thin curves show the adiabatic energies for the α and ^{3}He channels. In the thick curve, a local minimum appears around $S \sim 3$ fm, where the ^{5}He and ^{14}O nuclei strongly overlap to each other. This result means that the local minimum state corresponds to the $5p$–$2h$ states with the shell-model-like configuration.
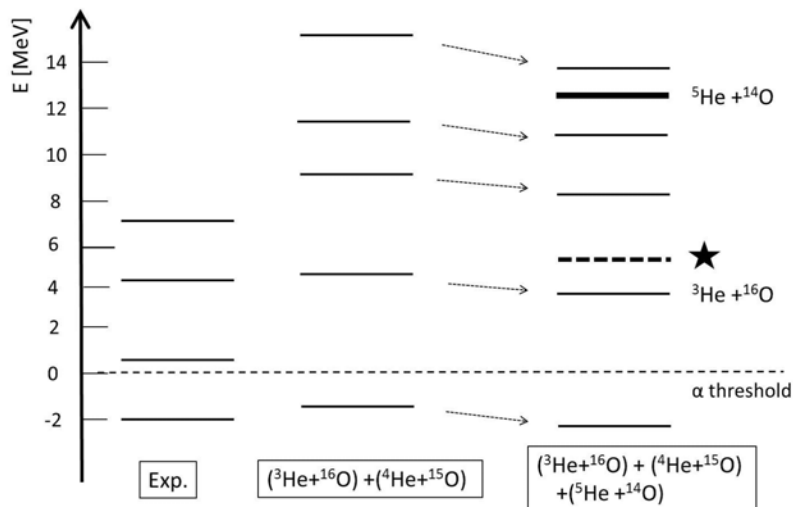

Figure 5. Energy spectra for the $3/2^+$ state. The left levels shows the experimental spectra of the $3/2^+$ state, while the middle and right spectra are the results of the microscopic calculation. The middle levels are the GCM solution of (^{3}He+^{16}O) + (α+^{16}O), while the right levels are the result of the (^{3}He+^{16}O) + (α+^{16}O) + (^{5}He+^{14}O) calculation. The arrows indicate the corresponding levels between the middle levels and the right levels. See text for details.

In the full calculation shown in the right panel, we find the further effect of other ^{5}He + ^{14}O channel. In the full calculation, the minimum point shifts to $S \leq 2$ fm, and the minimum energy of the full solution ($E_x \sim 13$ MeV with respect to the α threshold) is lower by about 10 MeV than the truncated calculation ($E_x \sim 23$ MeV). Therefore, the ^{5}He + ^{14}O correlation beyond the $5p$–$2h$ configuration is very important. However, the minimum energy in the full calculation is still higher by about 10 MeV than the threshold $3/2^+$ state ($E_x \sim 0.5$ MeV). On the contrary, the energy curves of $\alpha + ^{15}$O and ^{3}He + ^{16}O are almost unchanged after the full configurations of ^{5}He + ^{14}O is included. This result means that the coupling effects of the ^{5}He + ^{14}O channels are weak for the α and ^{3}He channels. Therefore, we can consider that the ^{5}He + ^{14}O configurations are basically decoupled from the coupled-channels model space of the two partitions, such as (^{3}He+^{16}O) + (α+^{15}O).

In order to see the difference of the theoretical calculation and experimental $3/2^+$ levels more clearly, we have performed the GCM calculation for the (^{3}He+^{16}O) + (α+^{16}O) + (^{5}He+^{14}O) coupled-channels. The energy spectra are shown in Fig. 5. In the calculation of (^{3}He+^{16}O) + (α+^{16}O) (middle

levels), there is only a bound $3/2^+$ state around the α threshold (dashed line), and no resonance appears around the threshold. On the contrary, a new levels with a dominant component of ^{5}He + ^{14}O appear around $E_x \sim 12$ MeV (thick level) in the extended calculation with the three partitions (right levels). However, the energy of the ^{5}He+^{14}O configuration is higher by about 10 MeV than the experimental $3/2^+$ state around the α threshold. The reason why the energy of the ^{5}He+^{14}O channel is too high is the incorrect reproduction of the threshold energy of the ^{5}He + ^{14}O channel in the theoretical calculation. The theoretical ^{5}He threshold is higher by about 7 MeV than the experimental threshold in the present setting of the nucleon-nucleon interaction. The ^{5}He nucleus is unbound with respect to the $\alpha + N$ threshold but this nucleus is handled by the simple HO wave function in the theoretical calculation. Therefore, the internal energy of the ^{5}He wave function is higher than the realistic ^{5}He nucleus.

Let us discuss the energy shift, which will arise from the correction of the threshold energy. If the ^{5}He threshold is correctly reproduced, the energy of ^{5}He+^{14}O will simply shift to the lower energy region by about 7 MeV, as shown by the dashed level with the star at the right level. Other levels will be unchanged even if the shift of the ^{5}He + ^{14}O level occurs. This is because of the de-coupling feature of ^{5}He + ^{14}O from the model space of the $(^3$He+^{16}O$) + (\alpha+^{15}$O$)$ coupled-channels. Therefore, the excitation energy of ^{5}He+^{14}O will be simply changed into $E_x \sim 5$ MeV with respect to the α threshold, (dashed level with the star). In this situation, the level repulsion is possible between the corrected ^{5}He+^{14}O state and the level at $E_x \sim 4$ MeV, which has a main component of ^{3}He + ^{16}O. Since the matrix element of the two neutron transfer is evaluated to be about $1 \sim 2$ MeV, the energy shift of the ^{3}He + ^{16}O state, which is generated from the perturbative coupling with ^{5}He + ^{14}O level, is estimated to be about -3 MeV. Therefore, there is a possibility that the $3/2^+$ state appear around the α threshold within the energy rang of about 1 MeV if the theoretical ^{5}He threshold is reproduced correctly. The reproduction of the ^{5}He threshold is important in the future calculation.

4 Summary and discussion

We have applied the microscopic and macroscopic cluster models to the ^{19}Ne nucleus and the energy levels are discussed. In the microscopic calculation, the coupled-channels calculation of $(^3$He+^{16}O$) + (\alpha+^{15}$O$)$ is performed on the basis of the generalized two-center cluster model (GTCM) [4]. In GTCM, the basis functions are constructed from the possible partitions of the valence neutrons around the ^{3}He and ^{14}O cores, and the anti-symmetrization among all the nucleons is completely taken into account. This model can produce the smooth connection of the weak coupling states and the strong coupling states in the adiabatic energy curves, which are the series of the energy eigenvalues as a function of the core distance.

In the small core distance, the strong coupling states are predominant, in which two nuclei are strongly overlapped with a specific geometrical configuration of the neutron hole. There are several local minima in the strong coupling region, and the strong coupling states are mainly included in the calculation of the generator coordinate method (GCM), in which the energy levels are calculated by superposing the distance parameter. The microscopic GCM calculation nicely reproduce the low-lying spectra below the α decay threshold. This result means the intrinsic character of the low-lying states are the strong coupling structure, in which the neutron hole is tightly bound inside of the α particle or the ^{16}O nucleus.

In the application of the macroscopic model, the $\alpha + ^{15}$O potential is speculated from the elastic scattering of the mirror system, $\alpha + ^{15}$N [12]. The resonant levels are calculated from the nuclear potential of $\alpha + ^{15}$N by imposing the absorbing boundary condition [19]. The potential model predicts the existence of the several resonances in both of the positive and negative parity states. These resonances will be observed in the excitation function of the resonant α scattering [20]. Therefore, the experimental identification by the α resonant scattering is interesting in future studies.

The present calculations do not reproduce the $3/2^+$ state, which is considered to have the main component of the $5p$–$2h$ shell model configuration [14]. The $5p$–$2h$ configuration corresponds to the ^{5}He + ^{14}O configuration in the shell model limit and hence, we have performed the extended microscopic calculation with the ^{5}He + ^{14}O configuration. The extended calculation suggests the formation of a new $3/2^+$ state, which has the dominant component of the ^{5}He+^{14}O channel, but its excitation energy is much higher than the experimental data. Since this failure about the $3/2^+$ energy is due to the incorrect reproduction of the theoretical ^{5}He threshold, the parameters of the nucleon-nucleon interaction must be revised to reproduce the ^{5}He threshold.

The exact treatment of all the threshold energies will be quite difficult in the microscopic approach because the internal structure of ^{3,4}He and ^{5}He is different; specifically, the former nuclei are tightly bound, while the ^{5}He is unbound nucleus with the $\alpha + N$ structure. In order to overcome this threshold problem, the semi-microscopic cluster model, the orthogonalized condition model (OCM) [11], is considered to be better approach than the full microscopic approach. In the OCM calculation, the threshold energies of all the open channels are handled in a phenomenological manner, in which the theoretical threshold energies to be set to the experimental value. Thus, the application of the OCM calculation will be effective to solve the problem the $3/2^+$ state just above the α threshold.

In the present study, we have combined the microscopic and macroscopic cluster model for the analysis of the low-lying bound and the highly-excited resonant states, respectively. However, the unified calculation from the bound states to the continuum states is an ideal study of the nuclear structure. Since the macroscopic model is difficult to consider the anti-symmetrization effect correctly, which is prominent in the low-lying bound states, the microscopic calculation should be applied to such the unified calculation. The analysis by the microscopic calculations is now underway.

References

[1] K. Ikeda et al., Prog. Theor. Phys. Suppl. **68**, 1 (1986).

[2] H. Horiuchi et al., Suppl. Prog. Theor. Phys. **192**, 1 (2012), and references therein.

[3] M. Freer, Rep. Prog. Phys. **70**, 2149 (2007).

[4] M. Ito and K. Ikeda, Rep. Prog. Phys. **77**, 096301 (2014).

[5] N. Itagaki, T. Otsuka, K. Ikeda and S. Okabe, Phys. Rev. Lett. **92**, 142501 (2004).

[6] Masaaki Kimura, Phys. Rev. C**75**, 034312 (2007).

[7] T. Yamada and Y. Funaki, Phys. Rev. C**82**, 064315 (2010).

[8] B. Buck and A. A. Pilt, Nucl. Phys. A**280**, 133 (1977).

[9] F. Nemoto and H. Bando, Prog. Theor. Phys. **47**, 1210 (1972).

[10] P. Descouvemont and D. Baye, Nucl. Phys. A**463**, 629, (1986).

[11] T. Sakuda and F. Nemoto, Prog. Theor. Phys. **62**, 1274 (1979).

[12] R. Otani et al., Phys. Rev. C**90**, 034306 (2014).

[13] K. Langanke et al., Astrophys. Jour. **301**, 629 (1986).

[14] Z. Q. Mao et al., Phys. Rev. Lett. **74**, 3760 (1995).

[15] H. Horiuchi, Suppl. Prog. Theor. Phys. **62**, 90 (1977).

[16] A. B. Volkov, Nucl. Phys. **74**, 33 (1965).

[17] N. Yamaguchi, T. Kasahara, S. Nagata, and Y. Akaishi, Prog. Theor. Phys. **62**, 1018 (1979).

[18] Andrá T. Kruppa, and K. Kato, Prog. Theor. Phys. **84**, 1145 (1990).

[19] Y. Takenaka et al., Prog. Exp. Theor. **2014**, 113D04 (2014).

[20] H. Yamaguchi et al., Phys. Rev. C**87**, 034303 (2013); H. Yamaguchi et al., Phys. Rev. C**83**, 034306 (2011).